Available online at www.sciencedirect.com
ScienceDirect
Journal of Organometallic Chemistry 692 (2007) 343–355
Journal of Organometallic Chemistry
www.elsevier.com/locate/jorganchem

Diiron(II) complexes showing a reversible oxygenation induced by a proton transfer mediated with a water molecule. Biological implication of a water molecule in hemerythrin function

Hidekazu Arii, Yasuhiro Funahashi, Tomohiro Ozawa, Koichiro Jitsukawa, Hideki Masuda *

Department of Applied Chemistry, Graduate School of Engineering, Nagoya Institute of Technology, Showa-ku, Nagoya 466-8555, Japan

Received 28 February 2006; accepted 24 April 2006
Available online 3 September 2006

Abstract

In our previous paper [J. Inorg. Biochem. (82) (2000) 153], diiron(II) complexes showing a reversible oxygenation have been reported as a functional model of hemerythrin (Hr) using a novel dinucleating polypyridine ligand with a hydroxyl OH group, *N*,*N*,*N*′,*N*′-tetrakis(6-pivalamido-2-pyridylmethyl)-1,3-diaminopropan-2-ol (HTPPDO). The ligand has formed two kinds of diiron(II) complexes with different structures, $[Fe^{II}_2(Htppdo)(PhCOO)](ClO_4)_3$ and $[Fe^{II}_2(tppdo)((p\text{-}Cl)PhCOO)](ClO_4)_2$, in which the former exhibited reversibility for dioxygen binding, while the latter was irreversible. Detailed reinvestigation of this interesting behavior has gave some first findings as follows; the reversible oxygenation of the diiron(II) complexes are induced by a proton transfer mediated with a water molecule rather than by higher redox potential of metal ion and higher hydrophobicity, which is an essential and important factor from a viewpoint of Hr function. The diiron(II) complexes employed here have been isolated as the following complexes, which were characterized crystallographically, spectroscopically, and electrochemically; $[Fe^{II}_2(Htppdo)((p\text{-}X)PhCOO)](ClO_4)_3$ (X = H, (**1**); OMe, (**2**); Cl, (**3**); NO_2, (**4**)) with which a hydroxyl proton of HTPPDO is retained, $[Fe^{II}_2(tppdo)((p\text{-}Cl)PhCOO)](ClO_4)_2$ (**5**) which has a deprotonated μ-alkoxide, and $[Fe^{II}_2(tpppn)((p\text{-}NO_2)PhCOO)](ClO_4)_3$(**6**) (TPPPN = *N*,*N*,*N*′,*N*′-tetrakis(6-pivalamido-2-pyridylmethyl)-1,3-diaminopropane) which has no such a hydroxyl group. The complexes **1**–**4** reacted with dioxygen in acetone solution containing small amount of water at −50 °C to give (μ-peroxo)diiron(III) complexes, which showed release of dioxygen by bubbling of Ar gas, although these complexes did not react with dioxygen in absolute acetone at all. The rate constants of the reactions of **1**–**4** with dioxygen indicated the Michaelis–Menten type saturation behavior for water concentration, indicating that the water molecule participates in the reversible dioxygen binding for **1**–**4**. These findings suggest that the proton transfer, which is induced by water as a mediator, is required for the reversible oxygenation with the diiron(II) complexes, which is the first proposal on biological significance of the proton transfer in oxygenation process of Hr and on the roles of a water molecule near μ-hydroxo oxygen in the active site of deoxyHr.

Keywords: Diiron complexes; Hydrogen bonds; Peroxo ligands; Proton transfer; Reversible oxygenation

1. Introduction

Biological organization is constructed by a precise control system in which a molecule recognizes the specific partner molecule. Non-covalent interactions, such as electrostatic, hydrophobic, van der Waals, and hydrogen bonding interactions, play very important role as the essential factors in the biological molecular recognition system, because their molecules need not only to associate but also to dissociate each other. Particularly, hydrogen bonding interaction is a key in maintaining of a structure of biological molecule, as seen in Watson–Crick base pairing in DNA and α-screw and β-sheet structures in proteins, and in appearing of protein functions [1]. In metalloproteins, hydrogen bond concerns to an interaction with an external molecule at the active site and to proton transfer pathway consisted of amino acid residues and water [2]. For example,

* Corresponding author. Tel./fax: +81 52 735 5228.
E-mail address: masuda@ach.nitech.ac.jp (H. Masuda).

0022-328X/$ - see front matter © 2006 Elsevier B.V. All rights reserved.
doi:10.1016/j.jorganchem.2006.04.052

in myoglobin (Mb), which storages oxygen molecule in muscle, the distal histidine interacts with two oxygen atoms of dioxygen molecule bound to heme iron. Recently, Watanabe et al. reported that the mutant of Mb, Mb(F43H/H64L), where the position of the distal histidine has been replaced by other amino acids, demonstrated a peroxidase-like activity [3], which indicates that hydrogen bonding interaction supports functions of metalloproteins. Also in oxyhemerythrin (oxyHr), one of non-heme diiron proteins and plays a role of dioxygen carrier in several marine invertebrate phyla [4–6], the hydrogen bond is seen between the bound hydroperoxide and μ-oxo oxygen, and it is supposed to participate in the reversible oxygenation. Such a hydrogen bonding interaction and the proton transfer behavior that are seen in Hr are very interesting, whose role and mechanism have never been clarified yet.

The crystal structure of deoxyhemerythrin (deoxyHr) revealed that the active site is consisted of two iron atoms having different coordination numbers; one iron site is a five-coordinate and another is a six-coordinate (Scheme 1) [7]. Dioxygen molecule binds to the coordinatively-unsaturated iron site in an end-on fashion as a hydroperoxide anion to generate oxyhemerythrin (oxyHr), accompanied by the two-electron reduction of dioxygen from diiron(II) core and one-proton acceptance from bridging μ-hydroxide (Scheme 1) [8–10]. The active site of Hr, as seen in those of many other metalloproteins, is surrounded by many hydrophobic amino acid residues, such as Leu, Ile, Phe, and Trp [7]. It has been reported that in myohemerythrin (MHr) which has the same function as Hr, their mutants with less hydrophobicity, MHr(L103V) and MHr(L103N), have exhibited faster autoxidations than the wild-type protein [11]. The hydrophobicity in dioxygen-transporting cavities of Hr and MHr is an important factor to prevent from autoxidation of the oxy types. Interestingly, we became aware that in two of four subunits for deoxyHr protein, water molecules have been found out near the active site with a distance of 2.7 Å from μ-hydroxide oxygen [10]. However, the authors do not have given any detailed discussion about presence and role of these water molecules.

In order to clarify the binding mechanism of dioxygen to the active centers of diiron proteins such as Hr and soluble methane monooxygenase, several diiron–peroxo complexes have been prepared through $Fe(II)_2/O_2$ [12–20] or $Fe(III)_2/H_2O_2$ [21–27] system. Most of the diiron model complexes prepared from the $Fe(II)_2/O_2$ system gave the corresponding peroxo complexes which dioxygen irreversibly coordinated to two irons in a μ-1,2 fashion, which were thermally unstable at room temperature. Kitajima et al. and Suzuki et al. independently succeeded in appearance reversible oxygenation using $[Fe^{II}(PhCOO)(MeCN)(HB(3,5\text{-}iPr_2pz)_3)]$ and $[Fe^{II}_2(Me_4-tpdp)(PhCOO)(H_2O)](BF_4)_2$, which demonstrated the reversibility at −20 °C and −40 °C, respectively [28–30]. Furthermore, Suzuki et al. improved the ligand and succeeded in preparation of a thermally stable diiron–peroxo species using diiron(II) complexes with sterically bulky ligands, $[Fe^{II}_2(Ph\text{-}bimp)(PhCOO)](BF_4)_2$, in which the complex $[Fe^{III}_2(Ph\text{-}bimp)(PhCOO)(O_2)](BF_4)_2$ was very stable at room temperature and showed reversible oxygenation [31]. Lippard et al. have recently reported that the diiron–peroxo complex prepared from the reaction of $[Fe^{II}_2(\mu-OH)(\mu-Ph_4DBA)(TMEDA)_2(OTf)]$ with O_2 demonstrated the UV–vis and resonance Raman spectra similar to oxyHr, but the formation of peroxo complex was irreversible, which is of importance as one of structural model complexes of Hr [32,33]. Considering that the redox potentials of the former diiron complexes coordinated with many nitrogen atoms are higher and those of the latter complexes coordinated with some oxygen atoms as well as nitrogen atoms are lower, the reversibility/irreversibility of oxygenation function in Hr model complexes may depend on the redox potentials of complexes.

Generally, it is thought that the reversible oxygenation in the model complexes is achieved by introduction of the iron ions that have been surrounded by hydrophobic environment and that have higher redox potentials. However, the structural information in Hr and oxygenation behaviors in the model systems brought the following three serious questions for us: (i) why is the two redox potentials of native Hr [34] (110 and 350 mV vs. NHE for Fe^{II}–O–Fe^{III}/Fe^{III}–O–Fe^{III} and Fe^{II}–OH–Fe^{II}/Fe^{II}–OH–Fe^{III}) rather lower than those of model complexes reported hitherto? [30,35], (ii) what is the role of a water molecule near μ-OH of diiron active center in deoxyHr? and (iii) what is the purpose of proton transfer of μ-OH in oxygenation process from deoxyHr to oxyHr? In the model systems, these factors are seemed to be unfavorable from a viewpoint of the dioxygen transport function, because the lower redox potential favors the formation of iron(III) than iron(II) and the water and/or μ-hydroxo protons lead the generated peroxo species to hydrogen peroxide or its decomposition.

Recently, we also succeeded in the preparation of function model of Hr, in which two kinds of diiron(II) complexes with reversibility and irreversibility were independently prepared using our originally designed ligand HTPPDO [36]. The diiron(II) complexes synthesized are $[Fe^{II}_2(Htppdo)(PhCOO)](ClO_4)_3$ (**1**) and $[Fe^{II}_2(tppdo)((p\text{-}Cl)PhCOO)](ClO_4)_2$ (**5**). The former showed the reversibility for oxygenation, while the latter was irreversible. The diiron complex with HTPPDO (**1**) exhibited lower redox potentials (292 and 790 mV vs. NHE under air) [36] in comparison with the model complexes reported hitherto [30,35].

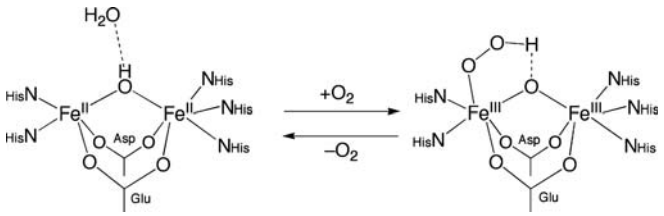

Scheme 1.

Our subsequent examination using the diiron complexes with HTPPDO gave quite important information in connection with essential factor on the reversible oxygenation in Hr: the reversible oxygenation is expressed by the proton transfer from μ-OH of deoxyHr to peroxide which has been induced by mediation of water. This behavior is also studied using the new dinucleating ligand without hydroxyl group, *N*,*N*,*N*′,*N*′-tetrakis(6-pivalamido-2-pyridylmethyl)-1,3-diaminopropane (TPPPN) (Scheme 2) as a comparison experiment. Here, we will describe and discuss the structure–function relationship on the reversible oxygenation in Hr, and concluded that the mobile proton and water molecule as a mediator as well as higher redox potential of diiron ions and hydrophobic environment around the active site are key factors.

2. Experimental

2.1. General procedure

All reagents used were of the highest grade available and were used without further purification. Ligand HTPPDO was synthesized according to the previously reported method [36]. *Caution: Perchlorate salts are potentially explosive and should be carefully treated!*

2.2. Synthesis of TPPPN

To a 1,4-dioxane solution (100 mL) containing the crude product 2-bromomethyl-6-pivalamidopyridine [37] (5.4 g, 0.020 mol) was added 1,3-diaminopropane (0.25 g, 3.4 mmol) and a NaOH (1.2 g, 0.022 mol) dissolved in water (10 mL). The solution was stirred for 1 day at room temperature, and then evaporated under reduced pressure. The residue dissolved in water was extracted by dichloromethane. The dichloromethane layer was dried over anhydrous $MgSO_4$ and evaporated under reduced pressure. The product was purified by silica gel column (eluent: ethylacetate). Yield: 0.75 g (27%). ^{1}H NMR ($CDCl_3$, 300 MHz): δ 1.31 (36H, s, *t*-Bu), 2.51 (4H, t, NCH_2), 3.62 (8H, s, NCH_2py), 7.10 (4H, d, py), 7.62 (4H, t, py), 8.09 (4H, s, NH) 8.11 (4H, d, py). FTIR (KBr, cm^{-1}): 3437, 2964, 1689, 1599, 1578, 1520, 1453, 1402, 1364, 1304, 1224, 1152, 803.

2.3. Syntheses of diiron(II) complexes

The preparation of diiron(III) complexes was carried out under Ar atmosphere in glove box as follows. The complexes, $[Fe^{II}_2(Htppdo)((p\text{-}X)PhCOO)](ClO_4)_3$ (X = H (**1**), OMe (**2**), Cl (**3**), NO_2 (**4**)) and $[Fe^{II}_2(tppdo)((p\text{-}Cl)PhCOO)](ClO_4)_2$ (**5**), were also prepared by the previously reported method [36].

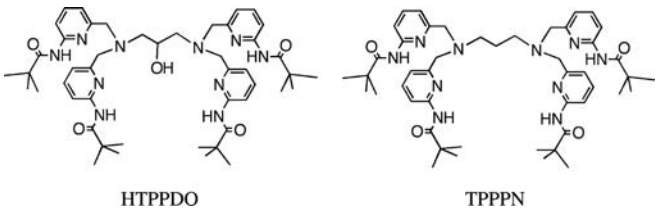

Scheme 2.

2.3.1. $[Fe^{II}_2(Htppdo)(PhCOO)](ClO_4)_3$ (*1*)

The preparation and characterization were previously described [33]. FTIR (KBr, cm^{-1}): 3350, 2971, 1655, 1617, 1531, 1463, 1421, 1303, 1217, 1087, 801, 728, 625.

2.3.2. $[Fe^{II}_2(Htppdo)((p\text{-}OMe)PhCOO)](ClO_4)_3$ (*2*)

60.4 mg (Yield 43%). Anal. Calc. for $\mathbf{2}\cdot H_2O$ ($C_{55}H_{75}Cl_3Fe_2N_{10}O_{21}$): C, 46.19; H, 5.29; N, 9.79. Found: C, 46.07; H, 5.18; N, 9.72%. FTIR (KBr, cm^{-1}): 3357, 2971, 1654, 1618, 1531, 1463, 1421, 1101, 800, 623.

2.3.3. $[Fe^{II}_2(Htppdo)((p\text{-}Cl)PhCOO)](ClO_4)_3$ (*3*)

116 mg (Yield 80%). Anal. Calc. for $\mathbf{3}\cdot H_2O$ ($C_{54}H_{72}Cl_4Fe_2N_{10}O_{20}$): C, 45.21; H, 5.06; N, 9.76. Found: C, 45.01; H, 4.96; N, 9.60%. FTIR (KBr, cm^{-1}): 3374, 2972, 1653, 1617, 1531, 1463, 1422, 1090, 801, 627.

2.3.4. $[Fe^{II}_2(Htppdo)((p\text{-}NO_2)PhCOO)](ClO_4)_3$ (*4*)

123 mg (Yield 85%). Anal. Calc. for $\mathbf{4}\cdot H_2O$ ($C_{54}H_{72}Cl_3Fe_2N_{11}O_{22}$): C, 44.88; H, 5.02; N, 10. 66. Found: C, 44.79; H, 4.98; N, 10.56%. FTIR (KBr, cm^{-1}): 3365, 2972, 1652, 1617, 1531, 1464, 1423, 1343, 1108, 799, 624.

2.3.5. $[Fe^{II}_2(tppdo)((p\text{-}Cl)PhCOO)](ClO_4)_2$ (*5*)

The preparation and characterization were previously described [36]. FTIR (KBr, cm^{-1}): 3369, 2967, 1668, 1613, 1562, 1528, 1461, 1404, 1159, 1088, 798, 624.

2.3.6. $[Fe^{II}_2(tpppn)((p\text{-}NO_2)PhCOO)](ClO_4)_3$ (*6*)

To a methanol solution (5 mL) of $Fe(ClO_4)_2\cdot 6H_2O$ (72.6 mg, 0.200 mmol) was added a mixture of TPPPN (83.5 mg, 0.100 mmol) and (*p*-NO_2)PhCOONa (18.9 mg, 0.100 mmol) in methanol (5 mL), which was stirred for 10 min. The standing of the reaction solution for several days gave a red crystal 130 mg (Yield 92%). Anal. Calc. for $\mathbf{6}\cdot 2H_2O$($C_{54}H_{80}Cl_3Fe_2N_{11}O_{22}$): C, 44.66; H, 5.42; N, 10.62. Found: C, 44.48; H, 5.11; N, 10.51%. FTIR (KBr, cm^{-1}): 3350, 1643, 1618, 1577, 1529, 1463, 1419, 1343, 1090, 625.

2.4. Measurements

Electronic absorption spectra were recorded on a JASCO V-570 spectrophotometer. Solid state IR spectra were measured on the KBr-disk method using a JASCO FT/IR-410 spectrophotometer, and solution state ones were recorded on AVATAR 360 FT-IR spectrophotometer using KRS-5 cell in acetonitrile at −40 °C under Ar gas. X-band ESR spectra were measured with a JEOL RE-1X spectrometer at 77 K. ^{1}H NMR spectral measurements were performed on a Gemini 300 MHz NMR spectrometer in $CDCl_3$ with TMS as an internal standard. Elemental

analysis was measured on a Perkin Elmer Japan 2440II CHNO/S corrected by acetoanilide. Electrochemical measurements were performed using a Bioanalytical Systems (BAS) CV-1B cyclic voltammetry unit anaerobically, with a three-electrode system consisting of a glassy carbon working electrode, a Pt-wire counter electrode and an Ag/Ag^+ reference electrode. All measurements were carried out at room temperature with a sweep rate of 100 mV s^{-1} under Ar in degassed distilled acetonitrile, using *n*-Bu_4NBF_4 as a supporting electrolyte. The electrochemical potentials were corrected by measurement of the ferrocene/ferrocenium couple.

2.5. X-ray crystallography

Single crystals of **1**–**6** suitable for X-ray diffraction analyses were obtained from their methanol solutions by standing for a few days under Ar atmosphere. Each crystal was mounted on a glass fiber, and the diffraction data were collected on a Rigaku/MSC Mercury CCD using graphite monochromated Mo Kα radiation at −100 °C. Crystal data and experimental details are listed in Table 1.

All the structures were solved by a combination of direct method and Fourier techniques, and all the non-hydrogen atoms were anisotropically refined by full-matrix least-squares calculations. Atomic scattering factors and anomalous dispersion terms were taken from the International Tables for X-ray Crystallography IV [38]. For all the crystals, since the numbers of reflection data were not enough to refine all the parameters of the hydrogen atoms, they were not included for further refinement; their positions were obtained from difference Fourier maps, except for a part of the hydrogen atoms of water molecules. All the calculations were carried out on a DELL computer by the Crystal Structure program [39].

2.6. Kinetics

The reaction rates of **1**–**4** with dioxygen were measured with a 1 cm path length quartz cell whose temperature was controlled at −50.0 °C by an Oxford thermostat (experimental error was ± 0.1 °C). The preparation of the diiron–peroxo species was monitored by following the increase in the absorption intensity at 610 nm. For the reaction condition of addition of excess dioxygen to diiron(II) complexes, where the concentration of **1**–**4** was 0.50 mM, the absorption change obeyed a first-order rate law. The data were analyzed with Delta Graph (Polaroid Computing) running on a Macintosh computer and fitted to an exponential function by non-linear least-squares method.

3. Results

3.1. Preparations and physico-chemical properties of *1*–*6*

Complexes **1**–**5** were prepared according to the previously reported methods [36], and complex **6** was synthe-

Table 1
Crystallographic data and experimental details for diiron(II) complexes **1**–**6**

	1 · 2MeOH	**2** · 2MeOH	**3** · 2MeOH	**4** · 2MeOH	**5** · MeOH	**6** · MeOH
Formula	$C_{56}H_{79}Cl_3Fe_2N_{10}O_{21}$	$C_{57}H_{81}Cl_3Fe_2N_{10}O_{22}$	$C_{56}H_{78}Cl_4Fe_2N_{10}O_{21}$	$C_{56}H_{78}Cl_3Fe_2N_{11}O_{23}$	$C_{55}H_{73}Cl_3Fe_2N_{10}O_{16}$	$C_{55}H_{74}Cl_3Fe_2N_{11}O_{21}$
Formula weight	1446.35	1476.37	1480.79	1491.35	1348.29	1443.30
Crystal system	Triclinic	Monoclinic	Monoclinic	Monoclinic	Orthorhombic	Monoclinic
Space group	$P\bar{1}$ (#2)	$P2_1/c$ (#14)	$P2_1/n$ (#14)	$P2_1/n$ (#14)	$Pna2_1$ (#33)	$P2_1/n$ (#14)
a (Å)	11.589(4)	11.430(3)	11.6131(5)	11.5764(5)	28.7524(11)	11.376(1)
b (Å)	14.870(4)	19.902(5)	19.815(1)	19.8197(8)	11.5909(5)	20.166(2)
c (Å)	19.687(6)	30.789(8)	30.036(2)	30.177(2)	18.3216(8)	30.0444(9)
α (°)	84.002(7)			–	–	–
β (°)	87.924(7)	99.741(4)	102.091(3)	101.585(3)	–	100.941(1)
γ (°)	80.398(6)			–	–	–
V (Å^3)	3326(1)	6902(3)	6758.3(6)	6782.8(5)	6106.0(4)	6767(1)
Z	2	4	4	4	4	4
ρ_{calcd} (g cm^{-3})	1.444	1.420	1.455	1.460	1.467	1.417
μ (Mo K_α) (mm^{-1})	6.36	6.15	6.66	6.28	6.81	6.25
Total number of data	26302	55194	54202	53817	48184	70943
Number of unique data	14568	15775	15256	15386	13336	15346
Observed data[a]	12445	11284	9013	11641	12813	7858
Number of parameters	903	923	847	938	845	899
R_1/wR_2[b]	0.074/0.161	0.088/0.196	0.073/0.140	0.085/0.186	0.050/0.112	0.089/0.213

[a] $I > 2\sigma \cdots$.
[b] $R_1 = \sum ||F_o| - |F_c|| / \sum |F_o|$. $wR_2 = \{\sum (w(F_o^2 - F_c^2)^2) / \sum w(F_o^2)^2\}^{1/2}$.

Table 2
Selected bond lengths (Å) for diiron complexes **1**–**6**

	1	**2**	**3**	**4**	**5**	**6**
Fe(1)···Fe(2)	4.974(1)	5.013(1)	4.999(1)	5.017(1)	3.722(1)	5.111(2)
Fe(1)–O(1)	2.325(3)	2.304(3)	2.254(4)	2.248(3)	2.057(2)	–
Fe(2)–O(1)	3.523(3)	3.568(3)	3.551(4)	3.559(3)	2.190(3)	–
Fe(1)–N(1)	2.278(3)	2.269(4)	2.266(4)	2.269(4)	2.298(3)	2.221(7)
Fe(2)–N(2)	2.274(3)	2.256(4)	2.255(4)	2.263(4)	2.346(3)	2.228(6)
Fe(1)–N(3)	2.321(3)	2.185(4)	2.198(4)	2.282(4)	2.300(3)	2.217(7)
Fe(1)–N(5)	2.198(3)	2.306(4)	2.289(4)	2.191(4)	2.357(3)	2.166(7)
Fe(2)–N(7)	2.164(3)	2.204(5)	2.214(5)	2.158(4)	2.278(3)	2.201(6)
Fe(2)–N(9)	2.199(3)	2.160(5)	2.155(5)	2.220(4)	2.384(3)	2.217(6)
Fe(1)–O(2)	2.125(3)	2.159(4)	2.154(4)	2.157(3)	2.075(2)	2.052(6)
Fe(1)–O(3)	2.167(3)	2.159(3)	2.151(4)	2.156(3)	2.244(3)	2.139(5)
Fe(2)–O(4)	2.139(3)	2.046(3)	2.030(4)	2.136(3)	2.212(2)	2.169(5)
Fe(2)–O(5)	2.072(3)	2.132(4)	2.129(4)	2.036(3)	2.164(2)	2.094(5)
Fe(1)–O(6)	2.082(2)	2.086(3)	2.126(3)	2.137(3)	2.093(2)	2.078(5)
Fe(2)–O(7)	2.082(3)	2.095(3)	2.106(4)	2.136(3)	2.131(2)	2.013(5)

sized by the method described in Section 2. The characterizations of these complexes were carried out by elemental and X-ray crystal structure analyses and UV–vis, IR, and ESR spectroscopies and CV measurement.

The electronic absorption spectra for **1**, **2**, **3**, **4**, **5**, and **6** in acetone solution exhibited intense bands at 404 nm ($\varepsilon = 1200\ M^{-1}\ cm^{-1}$), 396 nm ($\varepsilon = 1300\ M^{-1}\ cm^{-1}$), 395 nm ($\varepsilon = 1300\ M^{-1}\ cm^{-1}$), 407 nm ($\varepsilon = 1700\ M^{-1}\ cm^{-1}$), 419 nm (sh, $\varepsilon = 1000\ M^{-1}\ cm^{-1}$), and 420 nm ($\varepsilon = 1500\ M^{-1}\ cm^{-1}$), respectively, which were assigned to a MLCT of iron(II) to pyridine [40,41].

The solid state IR spectra gave intense bands characteristic of the C=O stretching vibration, ν(C=O), in the range of 1650–1655 cm^{-1} for **1**–**4**, at 1668 cm^{-1} for **5** and at 1643 cm^{-1} for **6**, all of which shifted toward a lower frequency region in comparison with metal-free HTPPDO (1688 cm^{-1}). These shifts imply the coordination of the carbonyl oxygens of ligand to iron, and the magnitude in these shifts can be well explained from the crystal structures of these complexes (see Table 2), as will be described at the next section; the strength of Fe–O(pivalamide) bonds becomes weaker in the order of **5** > **1**–**4** > **6**.

Electrochemical properties of complexes **1**–**6** were measured in an acetonitrile solution at room temperature anaerobically (Table 3 and Fig. S1). Redox potentials of complexes **1**–**4** exhibited two quasi-reversible redox waves, while the exact potential values for **5** and **6** were not obtained because they gave multi-oxidation waves that are difficult to analyze. The two half-wave potentials assignable to $Fe^{II}Fe^{III}/Fe^{III}Fe^{III}$ and $Fe^{II}Fe^{II}/Fe^{II}Fe^{III}$ couples were observed at 265 and 92 mV vs. Fc/Fc^{+} for **1**, at 266 and 78 mV for **2**, at 264 and 102 mV for **3**, at 295 and 127 mV (anode potential) for **4**, respectively. The value of $Fe^{II}Fe^{III}/Fe^{III}Fe^{III}$ couple was lower as compared with those of previously reported diiron complexes [30,35], which could be caused by raising the d-orbital energy levels of the iron ions by coordination of pivalamide oxygens of HTPPDO. Interestingly, these data clearly indicate that the $Fe^{II}Fe^{II}/Fe^{II}Fe^{III}$ couples have significantly been affected by *para*-substituent groups of bridging benzoate derivatives, although such an effect has not been observed for the $Fe^{II}Fe^{III}/Fe^{III}Fe^{III}$ couples; the redox potential values for the diiron complexes coordinated by benzoic acids with electron-withdrawing (**3**, **4**) and electron-donating groups (**2**) as *para*-substituent group, (*p*-X)$PhCOO^{-}$, are observed in higher and lower potential regions than that with $PhCOO^{-}$ (**1**), respectively. The above findings suggest that the benzoate ligand may remove the hydroxyl proton of HTPPDO to be released as benzoic acid from diiron core in the $Fe^{II}Fe^{III}/Fe^{III}Fe^{III}$ oxidation process (Scheme 3).

Table 3
Electrochemical properties of diiron complexes as measured anaerobically[a]

	$E_{1/2}(Fe^{II}Fe^{III}/Fe_2^{III})(\Delta E_p)$	$E_{1/2}(Fe_2^{II}/Fe^{II}Fe^{III})(\Delta E_p)$	ΔE[b]	Reference
1	265 (70)	92 (102)	173	[c]
2	266 (77)	78 (119)	188	[c]
3	264 (67)	102 (83)	162	[c]
4	295 (pa)	127 (67)	–	[c]
$[Fe_2^{II}(Me_4-tpdp)(PhCOO)(H_2O)]^{2+}$	455	65	390	[d]
$[Fe_2^{II}(Ph-tidp)(PhCOO)]^{2+}$	555	65	490	[e]
Hr	110	350	−240	[f]

[a] The electrochemical values (mV) represented here are vs. Fc/Fc^{+}.
[b] ΔE represents the difference from redox potential of $Fe^{II}Fe^{III}/Fe^{III}Fe^{III}$ to that of $Fe^{II}Fe^{II}/Fe^{II}Fe^{III}$.
[c] This work.
[d] Measured in CH_2Cl_2. Ref. [30].
[e] Measured in CH_2Cl_2. Ref. [35].
[f] Measured in water at pH 8.2 vs. NHE. Ref. [34].

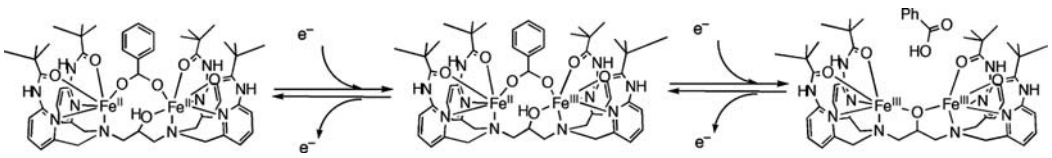

Scheme 3.

Furthermore, it is quite unique that the differences between the redox potential values of $Fe^{II}Fe^{III}/Fe^{III}Fe^{III}$ and $Fe^{II}Fe^{II}/Fe^{II}Fe^{III}$ couples for **1**–**4**, ΔE, are very close in comparison with those of diiron complexes reported hitherto [30,35,40–45]. The smaller ΔE values in complexes **1**–**4** must have been induced by the protonation/deprotonation of the OH group of HTPPDO. The redox potential values for Hr are 110 and 350 mV for $Fe^{II}Fe^{III}/Fe^{III}Fe^{III}$ and $Fe^{II}Fe^{II}/Fe^{II}Fe^{III}$ couples, respectively, and the ΔE value is negative (−240 mV), although those in diiron complexes and diiron proteins should generally be $Fe^{II}Fe^{III}/Fe^{III}Fe^{III} > Fe^{II}Fe^{II}/Fe^{II}Fe^{III}$. This unique behavior in Hr is interpreted in terms of the proton transfer phenomenon (Fe–OH–Fe → Fe–O–Fe). Diiron complexes that give larger ΔE value are stabilized at the oxidation state of Fe^{II}-Fe^{III} to disadvantage the reversible oxygenation, and the smaller value makes it smooth. A protonation/deprotonation of bridging hydroxo group affects a reversible oxygenation.

3.2. Crystal structures of *1*–*6*

All the single crystals of complexes **1**–**6** were obtained and analyzed by X-ray method. Complexes **1** and **5** were also reanalyzed and refined, although they were reported previously [36]. The crystal structures of the cation parts for complexes **1** and **6** are shown in Figs. 1 and 2, respectively. Since those for complexes **2**–**4** are essentially the same as that of **1** and complex **5** has been reported previously, their figures have been omitted. The selected bond lengths around the diiron cores for **1**–**6** are listed together in Table 2.

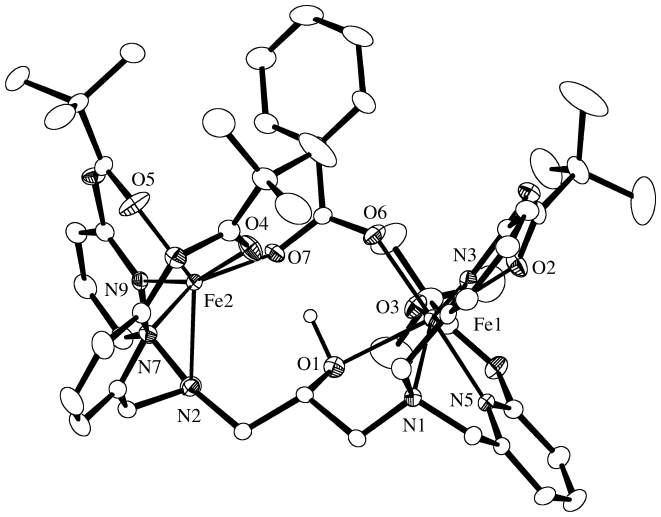

Fig. 1. Crystal structure of the cation part of **1**, showing 30% probability thermal ellipsoids. The hydrogen atoms except for the proton of alcohol group are omitted for clarity.

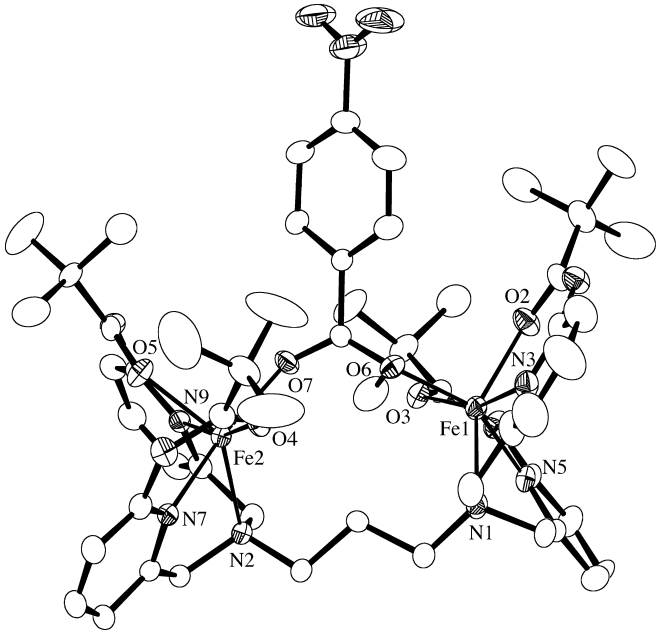

Fig. 2. Crystal structure of the cation part of **6**, showing 30% probability thermal ellipsoids. The hydrogen atoms are omitted for clarity.

The geometries around the two iron(II) ions for complexes **1**–**4** are asymmetric. The Fe(1) site has a seven-coordinate capped octahedron comprised of an N_3O_4 donor set which includes the hydroxyl oxygen of HTPPDO, and another Fe(2) center forms a six-coordinate distorted octahedron with an N_3O_3 donor set with a dioxygen-accessible vacant site. Although the two iron centers are bridged by benzoate, the hydroxyl oxygen of HTPPDO does not participate as the bridging ligand. These complexes showed longer Fe–N(pyridine) bond lengths (2.16–2.32 Å) as compared with the Fe–N(pyridine) bonds reported previously (2.10–2.25 Å) [46,47], as seen in Table 2. Interestingly, the hydroxyl proton of HTPPDO, as is apparent from the crystal structure of complex **1** (Fig. 1), has been left as it was. The hydroxyl oxygen linked to Fe(1) weakly with a distance of 2.325(3) Å and the hydroxyl proton attached to O(1) hydrogen-bonded to the carboxylate oxygen O(7) with the O(1)···O(7) distance of 2.653(4) Å and the angle of ∠O(1)–H–O(7) = 165(6)° (Table 4), which lies in the shortest side of the general hydrogen bond distances (2.6–3.2 Å) and is close to an ideal angle for a hydrogen bond. These results mean the formation of strong intramolecular hydrogen bond between the hydroxyl proton and

Table 4
Bond parameters showing intramolecular hydrogen bonding interaction for diiron complexes **1**–**4**

	O(1)–O(7) (Å)	O(1)–H (Å)	O(7)···H (Å)	∠O(1)–H–O(7) (°)
1	2.653(4)	1.18(7)	1.49(9)	165(6)
2	2.631(4)	1.04(11)	1.6(2)	160(10)
3	2.618(5)	1.039(4)	1.631(7)	156.6(3)
4	2.620(4)	1.18(12)	1.5(2)	158(7)

the carboxylate oxygen of benzoate derivatives. It is quite unique that the OH group of HTPPDO does not play as a bridging ligand, which is attributed to the steric repulsion between bulky pivalamide groups attached on six-position of pyridines. The coordination of benzoate to diiron ions for **1**–**4** is significantly influenced by the electronic effect of *para*-substituent groups of the benzoate derivatives; those with the electron-donating and electron-withdrawing substituent groups cause the bond lengths of Fe(1)–O(6) and Fe(2)–O(7) to shorten and lengthen, respectively (Table 2), and then the Fe(1)–O(1) bonds for **1**–**4** also indicated the reverse tendency reasonably. The strong coordination of carboxylate oxygen O(6) with Fe(1) that was induced by electron-donating *para*-substituent group will shorten the Fe(1)–O(6) bond, which will decrease the acidity of Fe(1) and then weaken the coordination of O(1) to Fe(1). These follow the Hammett's rule as shown in Fig. 3.

The structure of **5**, as described previously, revealed that the two iron ions have a capped octahedral geometry with N_3O_4 donor sets each other, and that both of hydroxyl oxygen of TPPDO and benzoate oxygens played a role of bridging ligand. The structure of **6**, in which the two iron ions are coordinated with N_3O_3 donor sets each other, was almost the same as those of **1**–**4** except for the absence of the bridging hydroxyl group. The shorter Fe(1)–O(6) and Fe(2)–O(7) bonds for **6**, as compared with those for **1**–**4,** might have been caused by lack of repulsion between their bulky *tert*-butyl groups because of the flexible diaminopropane backbone due to the absence of hydroxyl group.

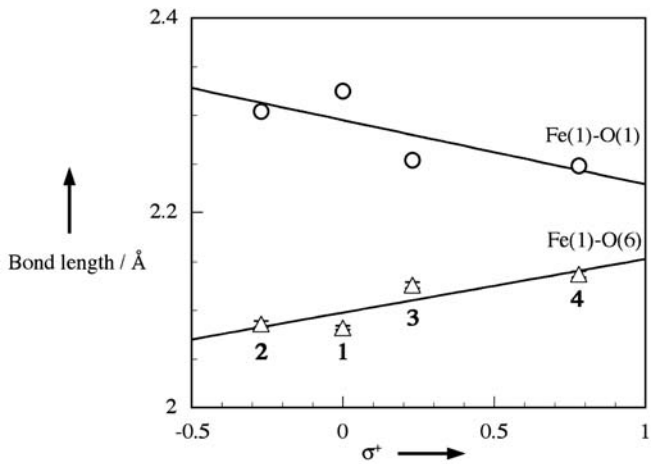

Fig. 3. Hammett plots of Fe(1)–O(1) and Fe(1)–O(6) bond lengths of **1**–**4** of vs. σ^+.

3.3. Electronic absorption, ESR and IR spectra in reactions of 1–6 with O_2

Reactions of complexes **1**–**4** with dioxygen in acetone solution showed two critical differences between in the presence and absence of water, although such a difference in reaction behaviors was not detected in the cases of complexes **5** and **6** as described below.

An exposure of dioxygen to an absolute acetone solution of **1** at −50 °C did not exhibit a remarkable spectral change, although a small broad band was observed in the range of 600–700 nm and the solution color changed slightly from yellow to greenish-yellow. It indicates that **1** does not react with dioxygen in absolute acetone. The small broad band observed, as is described below, might be attributable to the presence of slight amount of water that has been dissolving into the solution by the bubbling of dioxygen in spite of careful treatment. When 500 equivalents of water to **1** was added to its absolute acetone solution, the solution color turned vigorously from yellow to green, indicating the preparation of a peroxo species (**1**-O_2). Because the electronic absorption spectrum showed an intense band at 606 nm ($\varepsilon = 1800\ M^{-1}\ cm^{-1}$ per 2Fe) assignable to LMCT band of peroxo to iron(III), which is the same as the previously reported behavior [36]. The reactions of **2**, **3**, and **4** with dioxygen under the same condition also revealed the same spectral changes with the bands at 609 nm ($\varepsilon = 2000\ M^{-1}\ cm^{-1}$ per 2Fe), 606 nm ($\varepsilon = 1800\ M^{-1}\ cm^{-1}$ per 2Fe) and 603 nm ($\varepsilon = 1600\ M^{-1}\ cm^{-1}$ per 2Fe), respectively, as shown in Fig. 4 and Table 5. These characteristic bands disappeared by bubbling of Ar gas as soon as the solution was warmed from −50 °C to room temperature, which were reproduced by exposure to dioxygen at −50 °C. They exhibited reversibility by alternate bubbling of O_2 and Ar for all cases. Additionally,

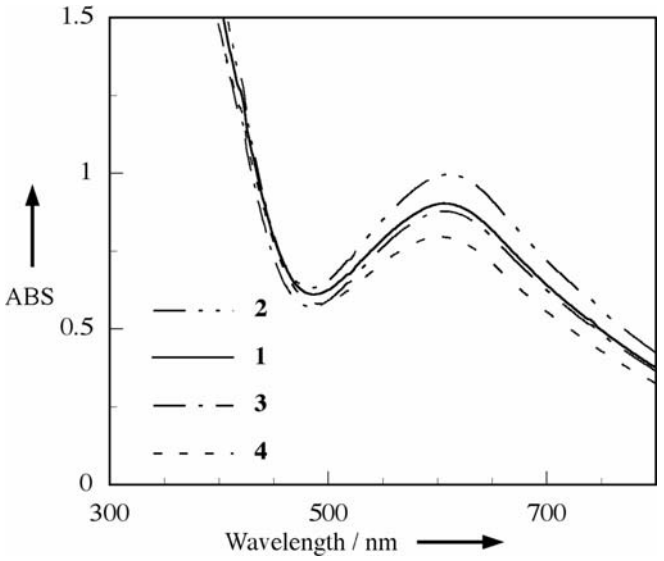

Fig. 4. Electronic absorption spectra of the peroxo adducts prepared from the reaction of **1**–**4** with dioxygen molecule at −50 °C in water-containing acetone solutions of **1**–**4**.

Table 5
Spectroscopic data and kinetic parameters for the reaction of diiron(II) complexes **1**–**4** with dioxygen at −50 °C in acetone

	λ_{max} (nm)	ε (M^{-1} cm^{-1})	K_M (M)	k'_{on} (10^{-3} s^{-1})
1	606	1800	0.18(1)	6.7(2)
2	609	2000	0.17(1)	6.3(2)
3	606	1800	0.12(1)	3.8(1)
4	603	1600	0.056(6)	2.81(5)

the reversible oxygenation reactions of **1**–**4** were exhibited in aprotic solvents such as acetonitrile, but not in protic solvent like methanol (Fig. S2), implying that an electrostatic interaction such as hydrogen bond relates to the reversible oxygenation. These findings indicate that the peroxo–diiron species generated from **1**–**4** are all almost the same ones. The subtle change in the λ_{max} values may be attributed to the electronic effect of the *para*-substituent group of benzoate derivatives. The magnitude in molar extinction coefficient might reveal the amounts of peroxo species generated. Considering that the coordination structures of the peroxo complexes derived from **1**–**4** are all the same, the benzoate derivatives with larger pK_a value, as will be described below, will appear higher deprotonation ability for the hydroxyl OH of HTPPDO to make the peroxo species generate effectively.

Reaction of complex **5** with dioxygen gave the color change from yellow to purple for both in absolute acetone and in water-containing acetone solution at −50 °C, whose electronic absorption spectra exhibited a broad band assignable to LMCT of peroxo to iron(III) at 550 nm ($\varepsilon = 1200$ M^{-1} cm^{-1} per 2Fe) for both cases. The difference in the spectral behaviors between **1**–**4** and **5** clearly indicates that the peroxo species generated are different. Moreover, the peroxo species derived from complex **5** did not show the release of dioxygen by bubbling of Ar even at ambient temperature.

For reaction of **6** with dioxygen, it did not show any spectral change both in absolute acetone and in water-containing acetone solution at −50 °C, and further it did not react with dioxygen even in the solution warmed to room temperature. It indicates that **6** does not react with dioxygen to be divalent just as they were.

ESR spectra of the reaction products of **1**–**4** and **5** with dioxygen, as measured in acetone at 77 K, were silent due to a strong antiferromagnetic coupling between two iron(III) atoms, suggesting that they prepared μ-peroxo adducts. Furthermore, the resonance Raman spectrum of the reaction products of **1**, as were described in the previous paper [36,48], supported the formation of peroxo species.

IR spectra of the peroxo species derived from complex **1** in MeCN at −40 °C revealed a new absorption band characteristic of C=O stretching vibration of benzoic acid at 1713 cm^{-1}, besides the C=O stretching vibrations from the pivalamide carbonyl groups were observed in the range of 1650–1655 cm^{-1} (Fig. 5C). The specific region of the C=O stretching vibration of the pivalamide carbonyl group did not show any drastic change between before and after the formation of peroxo adduct, indicating that all the amide oxygen atoms maintain the coordination with iron ions. The new C=O stretching vibration at 1713 cm^{-1} appeared in the same region as that of metal free benzoic acid measured in MeCN (Fig. 5D) [49,50]. These facts imply that the benzoate ligand bridging to the iron ions abstracts a proton to be liberated as benzoic acid. Interestingly, the spectral pattern of ν(C=O) stretching band in the peroxo complexes was different from those of metal free benzoic acid with two bands at 1713 and 1723 cm^{-1} which are observed as the equilibrium state between monomer and dimer molecule via intramolecular hydrogen-bonding interaction. Since the lower ν(C=O) band at 1713 cm^{-1} is attributed to that of hydrogen-bonding dimer, it is considered that the benzoic acid of the peroxo complex interacts by a hydrogen-bonding interaction with the other benzoic acid or the complex from which it liberates.

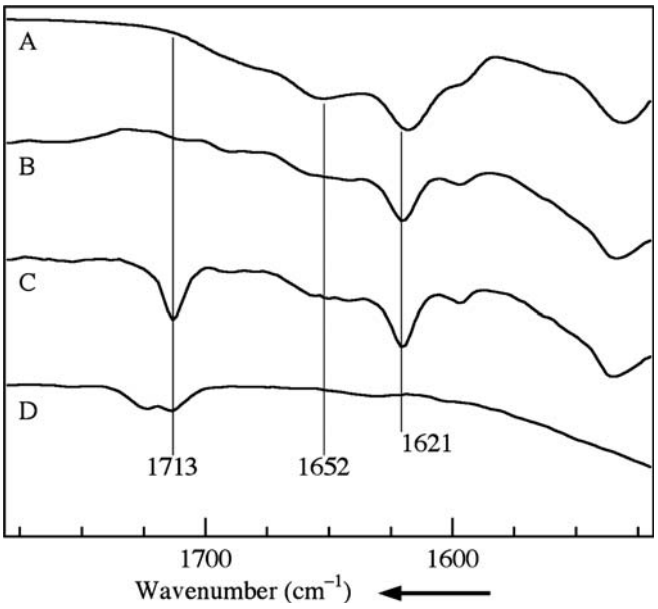

Fig. 5. Solution and solid state IR spectra in relation to the reaction of $[Fe^{II}_2(HTPPDO)(PhCOO)](ClO_4)_3$ (**1**) and O_2: $[Fe^{II}_2(HTPPDO)(PhCOO)](ClO_4)_3$ (**1**) in KBr pellet (A), and **1** in MeCN (B). The peroxo diiron(III) complex obtained by bubbling of O_2 into MeCN solution of B (C). PhCOOH in MeCN (D).

The above findings reveal that the reversible-binding of dioxygen molecule requires the hydroxyl group with mobile proton and a water molecule.

3.4. Kinetics for reactions of *1*–*6* with O_2

In order to elucidate the participation of water in binding with dioxygen, the kinetic study on binding rates of dioxygen with the diiron complexes were carried out on concentration dependence of water. The rate constant (k_{obs}) observed at the formation of peroxo adduct (**1**-O_2), as measured in the presence of excess oxygen molecule, obeyed a good first-order kinetics, which depended on the concentration of water [H_2O]. The plots of k_{obs} vs.

[H_2O], as shown in Fig. 6, demonstrated the Michaelis–Menten type saturation behavior, indicating that the dinuclear iron(II) complex **1** forms a certain association with water molecules before it reacts with O_2. The reaction of **1** with dioxygen under existence of water can be expressed with the following equations [51]

$$\mathbf{1} + H_2O \underset{k-1}{\overset{k1}{\rightleftarrows}} \mathbf{1}\cdots H_2O \quad (1)$$

$$\mathbf{1}\cdots H_2O + O_2 \overset{k_{on}}{\rightarrow} \mathbf{1} - O_2 \quad (2)$$

Since [O_2] is excess compared with [$\mathbf{1}\cdots H_2O$], the Eq. (3) is derived from the Eqs. (1) and (2) according to the Lineweaver–Burk equation [52],

$$\frac{[H_2O]}{k_{obs}} = \frac{[H_2O]}{k'_{on}} + \frac{K_M}{k'_{on}} \quad (3)$$

where K_M is the Michaelis constant and k'_{on} is a pseudo-first-order rate constant in the reaction of $\mathbf{1}\cdots H_2O$ with dioxygen. According to Eq. (3), the Michaelis constant for **1** was estimated to be 0.18(1) M, and the other complexes also exhibited similar values; 0.17(1), 0.12(1), and 0.056(6) M for **2**,**3**, and **4**, respectively (Table 5). The larger K_M value means that in formation of (μ-peroxo)diiron(III) complex, the diiron(II) complex requires much water so that the proton is easily transferred from hydroxyl group to benzoate. We can consider the following two schemes as the possible association type; (i) the complex that water molecule bound to the iron ion and (ii) the attractive interaction between water molecules and diiron core. From the results of IR spectra of **1**, it is supposed that the structure does not cause any remarkable change between at solid state and in MeCN solution (Fig. 5A and B), suggesting that the water molecule does not bind with irons but weakly interacts. As is clear from the Hammett plots of Fig. 7, Michaelis constants K_M were sensitively affected by the *para*-substitutent groups of benzoate derivatives; the constant K_M decreased in the diiron complex with the

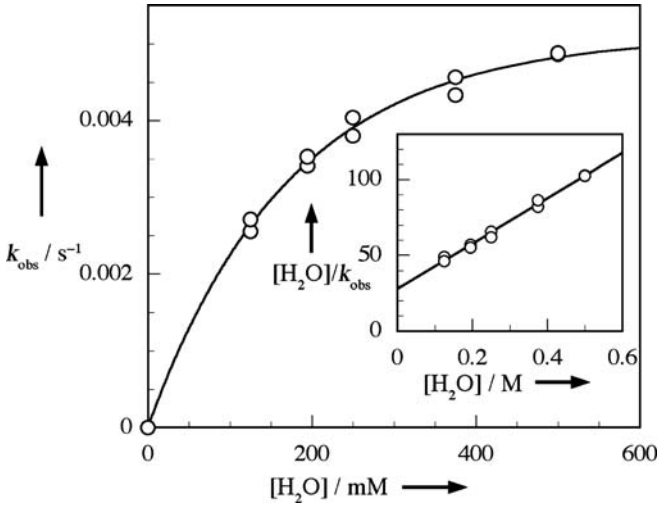

Fig. 6. Plots of the observed rate constants for generated amount of **1**-O_2 vs. concentration of H_2O in acetone at −50 °C. Inset: the double-reciprocal plot.

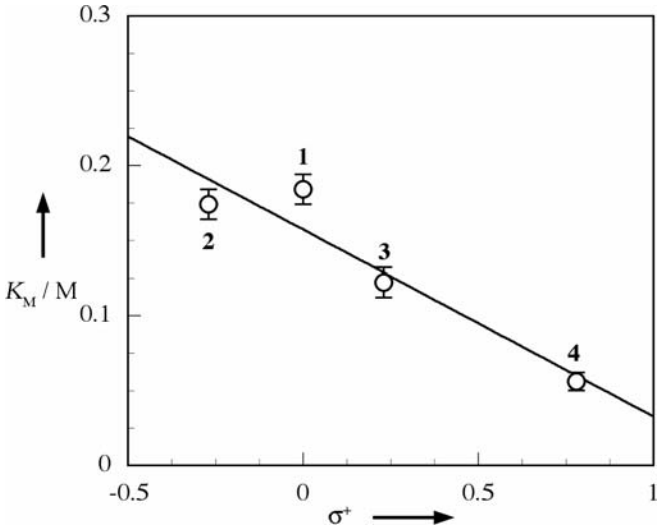

Fig. 7. Hammett plots of equilibrium constants in preparation of peroxo adducts vs. σ^+.

electron-withdrawing substituent group and increased in those with electron-donating group. Consequently, the interaction between the complex and water is supposed to occur at the position that the substituent effect of benzoate ligands sensitively appeared. As described above, such a tendency was also detected in the bond lengths Fe(1)–O(1, hydroxyl oxygen) and Fe(1)–O(6, benzoate oxygen) for the crystal structures of **1**–**4** (Fig. 3). Considering that complex **6** without the hydroxyl group was not affected by water for the reaction with dioxygen, the interaction sites of **1**–**4** with water are around the hydroxyl group. That is, the complex with benzoate derivatives having electron-withdrawing group does not need much water, because the proton transfer from O(1)H group to benzoate carboxylate is easily caused by the lower basicity of O(1) that was reduced by formation of stronger Fe(1)–O(1) bond. The k'_{on} values exhibited similar tendency, **1**,**2** > **3** > **4**: they are attributed to the pK_a values of benzoate derivatives that are affected by the abstraction of proton and/or the redox potentials of complexes. They became small in the diiron complexes with *para*-substituted benzoate ligand having a lower basicity (such as Cl (**3**) and NO_2 (**4**)), which increase the redox potential of the iron, and they became larger in those having a lower one (such as OMe (**2**)).

In order to examine the contribution of hydroxyl proton of HTPPDO ligand in the oxygenation for the diiron complexes, the pseudo-first-order rate constants of formation of the **1**-O_2 adduct were studied in the presence of H_2O and D_2O [53], which were estimated to be $3.86(15)\times10^{-3}$ and $3.35(9)\times10^{-3}$ s^{-1}, respectively. The kinetic isotope effect (KIE) value was 1.2. Since the KIE values of formation and dissociation of the peroxo adduct in Hr accompanied by proton transfer are 1.0 and 1.2, respectively [54], this value estimated here is quite appropriate. Therefore, the KIE value indicates that the proton transfer of hydroxyl group to benzoate includes in the rate-determining step in

the formation of the peroxo–diiron complex. Considering that the basicity of alcohol group is larger than that of benzoic acid, it is very interesting that the water mediates and promotes the proton transfer from hydroxyl group to benzoate. Here, we can claim that the water molecule compensates the proton through weak interaction with OH group, which assists the dissociation of hydroxyl proton.

4. Discussion

*4.1. Reaction mechanism for the reversible oxygenation in complexes **1–4***

From the above experimental results, the following three possible mechanisms are proposed for the reaction between the diiron complexes and dioxygen; (i) the benzoate is first removed as benzoic acid from the diiron complex, and then the dioxygen molecule reacts with diiron core, (ii) the dioxygen molecule attacks to the vacant site (Fe(2)) of diiron core, and then benzoate is released as benzoic acid, and (iii) the binding of dioxygen and release of benzoate ligand proceed simultaneously. However, the process (i) will be excluded from the IR spectral results that the benzoate of complex **1** is not removed in MeCN before dioxygen reacts with the irons. The process (ii) will also be removed by the experimental results that the complex **6** does not react with dioxygen, although it has a vacant site to be accessed by dioxygen. Consequently, it may be reasonable to consider that the binding of dioxygen and elimination of benzoic acid proceed simultaneously as follows (Scheme 4).

The O(1)H proton of HTPPDO of **1** in acetone solution containing water is in the situation of being easy to move. Such a condition will make the access of dioxygen to the vacant site of Fe(2) easy. Then the divalent Fe(2) atom will react with dioxygen to form an iron(III)-superoxo species, which are immediately continued by the transfer of O(1)H proton to the benzoate oxygen and the binding of deprotonated O(1) with Fe(2). The result that the benzoate has been liberated in the oxidation process from $Fe^{II}Fe^{III}$ to $Fe^{III}Fe^{III}$ agrees well with the finding that the redox potentials of $Fe^{II}Fe^{III}/Fe^{III}Fe^{III}$ couple, as described at the electrochemical results, are not affected by the electronic effect of *para*-substituted benzoate derivatives. The formation of μ-alkoxide will induce the electron transfer from divalent Fe(1) to trivalent Fe(2) through the Fe(2)–O–Fe(1) bond, next the extra electron on the Fe(2) will be transferred to superoxo to generate peroxo, and then the peroxide will immediately link to Fe(1). In the oxygenation, the benzoic acid that has once been released is required to be linked to the complex in order to maintain the reversibility, which may be understood from the IR spectrum of **1**-O_2 (Fig. 5C). Only one ν(C=O) band was detected at 1713 cm^{-1} for the oxygenated complex, which may suggest that the benzoic acid is not completely liberated. Because two ν(C=O) bands, corresponding to the monomeric and intermolecular hydrogen-bonded benzoic acids (Fig. 5D), must be observed if it was liberated as the benzoic acid.

4.2. Requirements in construction of model complex with reversible oxygenation function

In construction of the diiron model complex of Hr that can reversibly bind dioxygen, it is required that the diiron complex can form a thermally higher stable peroxo complex and easily turn between $Fe(II)_2$ and $Fe(III)_2$. The former was achieved by the diiron complex $[Fe^{II}_2$-(Ph-bimp)(PhCOO)$](BF_4)_2$ that the dioxygen molecule-bound space has been protected from attack of external ligands such as water by the sterically bulky hydrophobic groups [31]. The latter was performed by the diiron com-

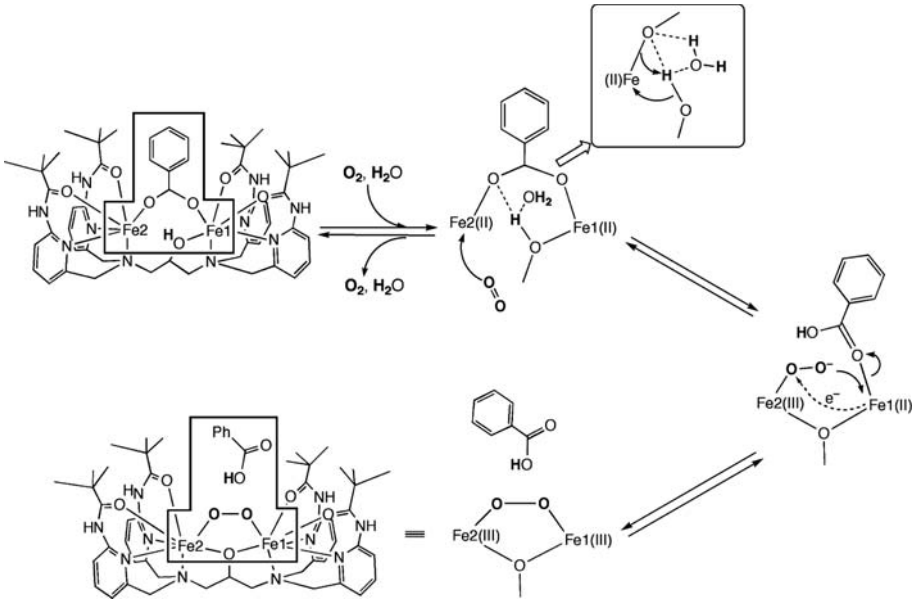

Scheme 4.

plex $[Fe^{II}_2(Me_4\text{-tpdp})(PhCOO)(H_2O)](BF_4)_2$ having the higher redox potentials (455, 65 mV vs. Fc/Fc^+) because of the weaker bond between the coordination atoms and iron [30]. However, the potentials of Hr are not so high (110, 350 mV vs. NHE). Here, there are three curious behaviors in Hr's function: (i) Hr exhibits reversible oxygenation in spite of its lower redox potentials. (ii) There is a water molecule near the diiron core with the distance of $O(H_2O)\cdots O(\mu\text{-OH}) = 2.7$ Å in deoxyHr. (iii) The μ-OH proton is transferred to peroxo in the oxygenation process of deoxyHr. At this stage, it is very interesting to clear the following questions; whether the higher redox potentials of the irons are required or not for reversible oxygenation? what is the role of the water molecule in deoxyHr? and why is the proton transferred from μ-OH to peroxide? We succeeded in the preparation of the diiron complexes having similar function to Hr, and the detailed examination gave very important aspects as follows.

(i) Complexes **1**–**4**, which have hydroxyl proton, do not react with dioxygen in absolute acetone, although they bind dioxygen reversibly in acetone solution containing a small amount of water. (ii) The benzoate anion coordinated to diiron was released as benzoic acid when dioxygen adduct was formed. (iii) Based on the kinetics experiments, it is clear that the proton of benzoic acid has been supplied from the hydroxyl proton of HTPPDO through mediation of water. (iv) It is also interesting that complex **5**, which does not have a hydroxyl proton, reacted with dioxygen to form peroxo species, regardless of the presence/absence of water. However, this peroxo species did not show the reversible oxygenation. (v) Complex **6**, which does not have the hydroxyl group, did not exhibit any reactivity for dioxygen, regardless of the presence/absence of the water. These facts indicate that the hydroxyl group having mobile proton is requested for the reversibility. (vi) Considering that the redox potentials of complexes **1**–**4** are lower in comparison with the diiron model complexes reported hitherto, although they are still higher than those of native Hr, the diiron core with higher redox potentials may not be required for the reversibility.

As described above, the reversible oxygenation in Hr's model complexes has been achieved not only by higher redox potentials of diiron ions and hydrophobic environment around the active center but also by the mobile proton from OH group and water molecule assisting the proton transfer. These structural features, needless to say, are attached also in Hr. Although only the higher redox potentials of irons and hydrophobicity around the active site have been discussed hitherto as the required conditions in construction of Hr's model complex, here we have first pointed out the roles and importance of the water and mobile proton in Hr.

4.3. Biological implication

Recently, the reaction scheme of reversible oxygenation in Hr has been proposed theoretically by Solomon and coauthors [55,56]. In this scheme, they have proposed the oxygenation scheme as follows: (i) the oxygenation is initially started by binding of O_2 to the open coordination site of the five-coordinated iron center of deoxyHr, (ii) the first electron transfer is carried out by the concerted proton-coupled electron transfer (ETPT) mechanism where the proton transfer from bridging hydroxo to the O_2 species and electron transfer from extra electron of another iron to π^*-orbital of the O_2 moiety through Fe–O–Fe mixed π/σ superexchange pathway proceed simultaneously, and (iii) finally the second electron transfer is induced by decrease of the $Fe\text{–}O_2H$ bond length. Here, based on our experimental results, we can propose the roles of bridging μ-OH ligand and a water molecule near its μ-OH group in deoxyHr: That is, the water molecule that links to bridging μ-OH by hydrogen-bond assists and promotes the proton transfer from μ-OH to peroxide. The smooth proton transfer mediated by a water molecule will assist Hr function, which might compensate the lower redox potentials of iron that is unfavorable for the reversible oxygenation.

Comparing with the crystal structures between deoxyHr and oxyHr [10], the water molecule detected near the active site of deoxyHr was not found out in that of oxyHr. It is sure that the small space of water in deoxyHr has been replaced by dioxygen.

5. Concluding remarks

In order to understand the mechanism of reversible oxygenation in Hr and to construct the Hr model complex with a low molecular weight, we have prepared some diiron complexes of sterically bulky hydrophobic polypyridine ligands with a hydroxyl group, **1**–**4**, and that with bridging μ-alkoxide oxygen, **5**, and that without such a hydroxyl group, **6**. They have been studied on the reactivity with dioxygen, and also examined on the effect of water. Then, the complexes **1**–**4** exhibited reversible oxygenation in acetone solution containing water, in which the rate constants of oxygenation depended on the concentration of water. However, they did not show any reactivity with dioxygen in absolute acetone. The complex **5**, which does not have a mobile hydroxyl proton, did not show reversibility, although it binds with dioxygen, and complex **6**, which does not have a hydroxyl group, did not exhibit even reactivity with dioxygen. These findings indicate that the reversible oxygenation in Hr is required to have the mobile proton and water molecule as its mediator rather than higher redox potentials of diiron ions and hydrophobic environment around the active site. Based on our experiments using the diiron complexes of HTPPDO, we succeeded in explaining the unique features in oxygenation function of Hr.

Acknowledgements

We thank Prof. Y. Watanabe of Nagoya University and Associate Professor S. Ogo of Osaka University for IR

spectral measurements. This work was supported partly by a Grant-in-Aid for Scientific Research (No. 11228203) from the Ministry of Education, Science, Sports, and Culture of Japan (H.M.) and supported in part by a Grant from the NITECH 21st Century COE Program (H.M.), to which our thanks are due.

Appendix A. Supporting information available

Cyclic voltammograms for **1**–**4**, UV–vis spectra on the reversible oxygenation of **1** in acetone, MeCN and MeOH. Supplementary data associated with this article can be found, in the online version, at doi:10.1016/j.jorganchem.2006.04.052.

References

[1] J.A. Cowan, in: Inorganic Biochemistry An Introduction, John Wiley and Sons, New York, 1997.
[2] A. Messerschmidt, R. Huber, T. Poulos, K. Wieghardt (Eds.), Handbook of Metalloproteins, vol. 1, John Wiley and Sons, West Sussex, 2001.
[3] S. Ozaki, T. Matsui, Y. Watanabe, J. Am. Chem. Soc. 119 (1997) 6666–6667.
[4] A. Feig, S.J. Lippard, Chem. Rev. 94 (1994) 759–805.
[5] S.J. Lippard, J.M. Berg, in: Principles of Bioinorganic Chemistry, University of Science, Mill Valley, 1994.
[6] E.I. Solomon, T.C. Brunold, M.I. Davis, J.N. Kemsley, S.-K. Lee, N. Lehnert, F. Neese, A.J. Skulan, Y.-S. Yang, J. Zhou, Chem. Rev. 100 (2000) 235–349.
[7] M.A. Holms, I. Le Trong, S. Turley, L.C. Sieker, R.E. Stenkamp, J. Mol. Biol. 218 (1991) 583–593.
[8] D.M. Kurtz Jr., D.F. Shriver, I.M. Klotz, J. Am. Chem. Soc. 98 (1976) 5033–5035.
[9] A.K. Shiemke, T.M. Loehr, J. Sanders-Loehr, J. Am. Chem. Soc. 106 (1984) 4951–4956.
[10] R.E. Stenkamp, Chem. Rev. 94 (1994) 715–726.
[11] G.M. Raner, L.J. Martins, W.R. Ellis Jr., Biochemistry 36 (1997) 7037–7043.
[12] Y. Dong, S. Ménage, B.A. Brennan, T.E. Elgren, H.G. Jang, L.L. Pearce, L. Que Jr., J. Am. Chem. Soc. 115 (1993) 1851–1859.
[13] Y. Dong, S. Yan, V.G. Young Jr., L. Que Jr., Angew. Chem. Int. Ed. Engl. 35 (1996) 618–620.
[14] J.R. Hagadorn, L. Que Jr., W.B. Tolman, J. Am. Chem. Soc. 120 (1998) 13531–13532.
[15] D.D. LeCloux, A.M. Barrios, T.J. Mizoguchi, S.J. Lippard, J. Am. Chem. Soc. 120 (1998) 9001–9014.
[16] S.V. Kryatov, E.V. Rybak-Akimova, V.L. MacMurdo, L. Que Jr., Inorg. Chem. 40 (2001) 2220–2228.
[17] E.Y. Tshuva, D. Lee, W. Bu, S.J. Lippard, J. Am. Chem. Soc. 124 (2002) 2416–2417.
[18] M. Enomoto, T. Aida, J. Am. Chem. Soc. 124 (2002) 6099–6108.
[19] D. Lee, B. Pierce, C. Krebs, M.P. Hendrich, B.H. Huynh, S.J. Lippard, J. Am. Chem. Soc. 124 (2002) 3993–4007.
[20] F.A. Chavez, R.Y.N. Ho, M. Pink, V.G. Young Jr., S.V. Kryatov, E.V. Rybak-Akimova, H. Andres, E. Münck, L. Que Jr., W.B. Tolman, Angew. Chem. Int. Ed. 41 (2002) 149–152.
[21] L. Westerheide, F.K. Müller, R. Than, B. Krebs, J. Dietrich, S. Schindler, Inorg. Chem. 40 (2001) 1951–1961.
[22] S. Ménage, J.-B. Galey, J. Dumats, G. Hussler, M. Seité, I.G. Luneau, G. Chottard, M. Fontecave, J. Am. Chem. Soc. 120 (1998) 13370–13382.
[23] R. Than, A. Schrodt, L. Westerheide, R. van Eldik, B. Krebs, Eur. J. Inorg. Chem. (1999) 1537–1543.
[24] M. Kodera, Y. Taniike, M. Itoh, Y. Tanahashi, H. Shimakoshi, K. Kano, S. Hirota, S. Iijima, M. Ohba, H. Okawa, Inorg. Chem. 40 (2001) 4821–4822.
[25] H. Hummel, Y. Mekmouche, C. Duboc-Toia, R.Y.N. Ho, L. Que Jr., V. Schünemann, F. Thomas, A.X. Trautwein, C. Lebrun, M. Fontecave, S. Ménage, Angew. Chem. Int. Ed. 41 (2002) 617–620.
[26] C. He, A.M. Barrios, D. Lee, J. Kuzelka, R.M. Davydov, S.J. Lippard, J. Am. Chem. Soc. 122 (2000) 12683–12690.
[27] É. Balogh-Hergovich, G. Speier, M. Réglier, M. Giorgi, E. Kuzmann, A. Vértes, Eur. J. Inorg. Chem. (2003) 1735–1740.
[28] N. Kitajima, N. Tamura, H. Amagai, H. Fukui, Y. Moro-oka, Y. Mizutani, T. Kitagawa, R. Mathur, K. Heerwegh, C.A. Reed, C.R. Randall, L. Que Jr., K. Tatsumi, J. Am. Chem. Soc. 116 (1994) 9071–9085.
[29] K. Kim, S.J. Lippard, J. Am. Chem. Soc. 118 (1996) 4914–4915.
[30] Y. Hayashi, T. Kayatani, H. Sugimoto, M. Suzuki, K. Inomata, A. Uehara, Y. Mizutani, T. Kitagawa, Y. Maeda, J. Am. Chem. Soc. 117 (1995) 11220–11229.
[31] T. Ookubo, H. Sugimoto, T. Nagayama, H. Masuda, T. Sato, K. Tanaka, Y. Maeda, H. Okawa, Y. Hayashi, A. Uehara, M. Suzuki, J. Am. Chem. Soc. 118 (1996) 701–702.
[32] T.J. Mizoguchi, S.J. Lippard, J. Am. Chem. Soc. 120 (1998) 11022–11023.
[33] T.J. Mizoguchi, J. Kuzelka, B. Spingler, J.L. DuBois, R.M. Davydov, B. Hedman, K.O. Hodgson, S.J. Lippard, Inorg. Chem. 40 (2001) 4662–4673.
[34] F.A. Armstrong, P.C. Harrington, R.G. Wilkins, J. Inorg. Biochem. 18 (1983) 83–91.
[35] H. Sugimoto, T. Nagayama, A. Maruyama, S. Fujinami, Y. Yasuda, M. Suzuki, A. Uehara, Bull. Chem. Soc. Jpn. 71 (1998) 2267–2279.
[36] H. Arii, S. Nagatomo, T. Kitagawa, T. Miwa, K. Jitsukawa, H. Einaga, H. Masuda, J. Inorg. Biochem. 82 (2000) 153–162.
[37] M. Harata, K. Hasegawa, K. Jitsukawa, H. Masuda, H. Einaga, Bull. Chem. Soc. Jpn. 71 (1998) 1031–1038.
[38] J.A. Ibers, W.C. HamiltonInternational Tables for X-ray Crystallography, vol. IV, Kynoch Press, Birmingham, UK, 1974.
[39] CrystalStructure: Crystal Structure Analysis Package, version 3.00, Rigaku and Rigaku/MSC, 2000–2002.
[40] A.S. Borovik, V. Papaefthymiou, L.F. Taylor, O.P. Anderson, L. Que Jr., J. Am. Chem. Soc. 111 (1989) 6183–6195.
[41] E. Lambert, B. Chabut, S. Chardon-Noblat, A. Deronzier, G. Chottard, A. Bousseksou, J.-P. Tuchagues, J. Laugier, M. Bardet, J.-M. Latour, J. Am. Chem. Soc. 119 (1997) 9424–9437.
[42] W. Kanda, W. Moneta, M. Bardet, E. Bernard, N. Debaecker, J. Laugier, A. Bousseksou, S. Chardon-Noblat, J.-M. Latour, Angew. Chem. Int. Ed. 34 (1995) 588–590.
[43] H. Nie, S.M.J. Aubin, M.S. Mashuta, C.-C. Wu, J.F. Richardson, D.N. Hendrickson, R.M. Buchanan, Inorg. Chem. 34 (1995) 2382–2388.
[44] M.G. Ghiladi, K.B. Jensen, J. Jiang, C.J. McKenzie, S. Morup, J. Ulstrup, J. Chem. Soc., Dalton Trans. (1999) 2675–2681.
[45] C. He, S.J. Lippard, Inorg. Chem. 40 (2001) 1414–1420.
[46] Y. Zang, J. Kim, Y. Dong, E.C. Wilkinson, E.H. Appelman, L. Que Jr., J. Am. Chem. Soc. 119 (1997) 4197–4205.
[47] M. Costas, C.W. Cady, S.V. Kryatov, M. Ray, M.J. Ryan, E.V. Rybak-Akimova, L. Que Jr., Inorg. Chem. 42 (2003) 7519–7530.
[48] The O–O stretching vibration, ν(O–O), for 1-O_2 was observed at 871 and 886 cm^{-1} which shifted to 825 and 836 cm^{-1} when using $^{18}O_2$ instead of $^{16}O_2$.
[49] R.H. Gillette, J. Am. Chem. Soc. 58 (1936) 1143–1144.
[50] Fig. 5D: Two bands at 1713 and 1723 cm^{-1} observed in acetonitrile at −40 °C were assigned to C=O stretching vibration of benzoic acid. At room temperature, the band at 1713 cm^{-1} disappeared and that at 1723 cm^{-1} remained, which indicate that the band of 1713 cm^{-1} is attributed to an intermolecular interaction of benzoic acid.

[51] A.L. Feig, M. Becher, S. Schindler, R. van Eldik, S.J. Lippard, Inorg. Chem. 35 (1996) 2590–2601.
[52] S. Itoh, H. Kumei, M. Taki, S. Nagatomo, T. Kitagawa, S. Fukuzumi, J. Am. Chem. Soc. 123 (2001) 6708–6709.
[53] An ESI-Mass spectrum of 1 in acetone containing D_2O exhibited a parent peak at $m/z = 362.7$ as a trivalent cation. Based on the calculation value for $[Fe^{II}_2(Htppdo)(PhCOO)]^{3+}$ at 361.1, it has been confirmed that the hydrogen atoms of the hydroxyl and four pivalamide groups of HTPPDO were replaced to deuterium ones.
[54] G.D. Armstrong, A.G. Sykes, Inorg. Chem. 25 (1986) 3135–3139.
[55] T.C. Brunold, E.I. Solomon, J. Am. Chem. Soc. 121 (1999) 8277–8287.
[56] T.C. Brunold, E.I. Solomon, J. Am. Chem. Soc. 121 (1999) 8288–8295.